

Atomic Force Microscopy Study of Biaxially-Oriented Polypropylene Films

H.-Y. Nie, M.J. Walzak, N.S. McIntyre
Surface Science Western
Room G-1, Western Science Centre
The University of Western Ontario
London, Ontario N6A 5B7, Canada

Abstract

Atomic force microscopy (AFM) uses a very sharply pointed mechanical probe to collect real-space morphological information of solid surfaces. AFM was used to image the surface morphology of a biaxially-oriented polypropylene film. The polymer film is characterized by a nanometer-scale fiber-like network structure, which reflects the drawing process used during the fabrication of the film. Polymer surface treatment to improve wettability by exposing the polymer to ozone with or without UV irradiation was studied using AFM. Surface morphology changes observed by AFM are the result of the surface oxidation induced by the treatment. Because of the topographic features of the polymer film, we have used the fiber-like structure to check the performance of the AFM tip. An AFM image is basically a mixture of the surface morphology and the shape of the AFM tip. Therefore, it is important to check the performance of a tip to ensure that the AFM image collected reflects the true surface features of the sample rather than contamination on the AFM tip.

Keywords: Atomic force microscopy (AFM); Biaxially-oriented polypropylene (BOPP); Surface morphology; UV/ozone treatment; AFM tip effect; Check tip performance using BOPP

Introduction

Scanning probe microscopy (SPM) is a relatively new family of microscopy that can measure surface morphology. SPM originated from the scanning tunnelling microscopy (STM)^{1,2}, in which electrical current caused by the tunnelling of electron through the tip and sample is used to maintain the distance between them. Because STM requires that the sample surface be conductive, atomic force microscopy (AFM)³ was developed in 1986 to measure insulating surfaces. AFM has since developed very rapidly and has found various applications in many fields.

AFM provides a real-space three-dimensional (3-D) image of a surface through the detection of an interaction between a sharp mechanical tip and the surface features. Dependent on

the operation mode of AFM, the interaction can be a contact force or an oscillation amplitude, which is used as the feedback parameter to adjust the distance between the tip and the sample surface. The tip scans the sample surface and the height information is obtained through the adjustment of the distance between them in order to keep the interaction constant. This technique requires almost no sample preparation and is able to obtain atomic spatial resolution.

Polypropylene (PP) is widely used in various areas from, for example, packaging to film capacitor. There have been reports of spherulitic structures on PP studied with scanning electron microscopy⁴ and transmission electron microscopy.^{5,6} AFM has been used to examine crystalline PP⁶⁻⁸ and nanometer-scale fiber formation on shear-deformed isotactic⁹ and hard elastic¹⁰ PP surfaces. Recently, studies on improving surface wettability on PP films using various surface modification techniques have been reported.^{11,12}

We have extensively studied the morphology of a biaxially-oriented polypropylene (BOPP) film using AFM.¹³⁻¹⁹ The surface morphology of the BOPP film is characterized by a fiber-like network structure.¹⁶ The nanometer-scale structure reflects the drawing process for fabricating the polymer film. AFM was also used to study changes in morphology and improvements in wettability caused²⁰⁻²² by exposing BOPP films to ozone with or without the presence of UV irradiation. Oxidation occurring on BOPP surfaces exposed to ozone alone is much slower than that introduced by the combination of ozone exposure and UV irradiation,^{20,22} which provides an opportunity to monitor the difference in the speed of oxidation between a "normal" (i.e., untouched) BOPP surface and a scratched surface. We have shown that the scratched surface has a higher¹⁵ surface energy than the "normal" surface and indicated a preferential oxidation¹⁷ on the scratched area. We show in this paper that preferential oxidation is more clearly observed in the scratched area when exposed to ozone alone.

In the course of studying the BOPP film, we realized that its morphology could be used to check the integrity of the AFM tip.^{18,19} An AFM image is, due to its imaging mechanism, a convolution of the tip geometry and the surface features. The sharper of either the AFM tip apex or the surface features acts

as the effective probe. Tip effect is defined as a situation where the geometry of tip dominates the AFM image. It is thus necessary for one to check how accurately an AFM image reflects the surface features of the sample. Metal films and many other materials have been used to characterize AFM tips.²³ The advantage of using a polymer film instead of those materials lies in the fact that the polymer surface is hydrophobic²⁴⁻²⁶ and soft²⁷ as compared to silicon²⁸⁻³⁰ AFM tips. These two properties are important for characterizing an AFM tip because they ensure that it is unlikely that the tip is contaminated or damaged in the verification process. Our ability to collect AFM images in the same area on the BOPP film surface before and after a contaminated tip was cleaned allows¹⁹ us to test the blind reconstruction³¹⁻⁴² algorithm, by which tip geometry can be extracted solely from the image it collected.

Materials

Thermally extruded, biaxially-oriented isotactic polypropylene film (3M Company) was used in this study. The BOPP film (0.03 mm thick) was produced from a homopolymer resin (molecular weight $M_w=1.9 \times 10^5$, polydispersity=6.0). The base resin contains 500-1000 ppm each of an inorganic acid scavenger and a high-molecular-weight phenolic antioxidant. The polymer was produced on a tenter frame film line and quenched at 45 °C prior to orientation. The film was formed with machine-draw (MD) and transverse-draw (TD) ratios of 5.2:1 and 9:1, respectively.

A sputtering system (Hummer VI, Technics EMS. Inc.) was used to coat ~ 30 nm thick gold film on a BOPP film for the purpose of checking how a metal coating alters the morphology of the polymer surface.

In order to replicate “native” scratches seen on the BOPP film, local mechanical stresses (scratches) were created using a stylus-type surface profiler (P-10, Tencor), in which a diamond tip having a radius of 2.5 μm was used to scan the film surface at a scan speed of 400 μm/s and a loading force of 0.4 mN. Variable forces of 0.1-0.5 mN were used to produce scratches with different widths.

BOPP films were treated by exposure to ozone flow (2×10^{17} molecule/cm³) with and without the presence of a UV irradiation with primary lines at 184.9 and 253.7 nm. The flow rate of the ozone-containing air stream was 1000 sccm (standard cubic centimeters per minute) for UV/ozone treatment and 5000 (or 2000 as specified where applicable) sccm for the ozone only treatment. Atomic oxygen formed from the photo-decomposition of ozone in the presence of 253.7 nm UV irradiation is believed to be the main reactant resulting in oxidation and eventual scission of BOPP molecular chains.²⁰ Because of the lack of atomic oxygen in the ozone only treatment, it has a much slower oxidation process compared with the UV/ozone treatment.

Methods

TopoMetrix’s AFM (Explorer) was employed in this study. A sharp tip formed on the free end of a cantilever is used to probe the sample surface. The interaction between the tip and the surface is detected by measuring the deflection of the cantilever using a laser diode to radiate the cantilever and a photodiode to detect the reflected laser beam. The quadrant photodiode is able to measure both the deflection and torsion of the cantilever. The principle of AFM is shown in Figure 1.

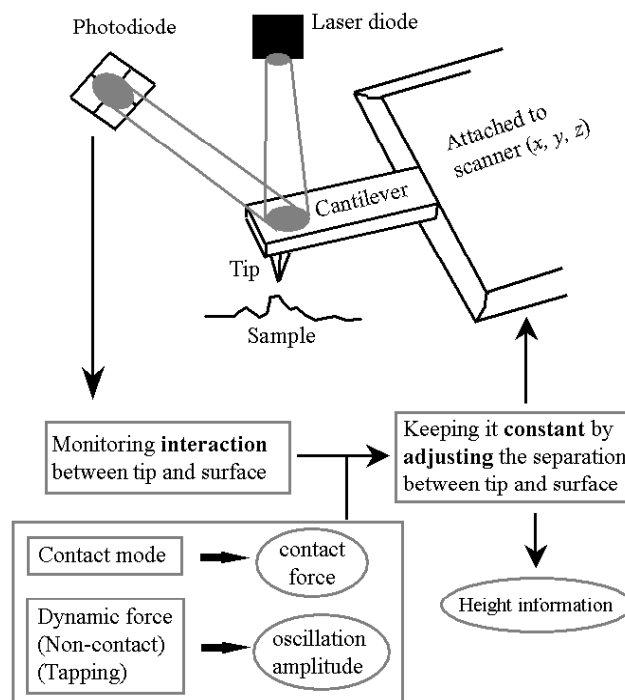


Figure 1: Schematic illustration of AFM principle: while scanning the tip across the sample surface (x, y), the system adjusts the distance (z , which is thus the measure of the height of the sample surface features) between the tip and the sample surface to maintain a constant contact force (contact mode) or oscillation amplitude (dynamic force mode). A 3-D image is thus constructed by the lateral dimension the tip scans and the height the system measures.

Shown in Figure 1 is the case where the tip scans the sample surface. The AFM operates by keeping constant the interaction between the tip and sample surface through a feedback system that adjusts the distance between the tip and the sample surface. Depending on the interaction between the tip and sample surface, which is used as the feedback signal, there are two different imaging modes described as follows.

Contact mode

In the contact mode AFM, the tip is in mechanical contact with the sample surface at a certain applied force. This applied force can be estimated from a force-distance curve, which is obtained by extending the tip to the surface to make

contact between the tip and the surface followed by retracting the tip from the surface. Shown in Figure 2 is a force-distance curve obtained using a soft silicon nitride cantilever (spring constant: ~ 0.03 N/m). The cantilever was $0.6 \mu\text{m}$ thick, $18 \mu\text{m}$ wide and $200 \mu\text{m}$ long with an attached tip whose apex radius was nominally 20 nm .

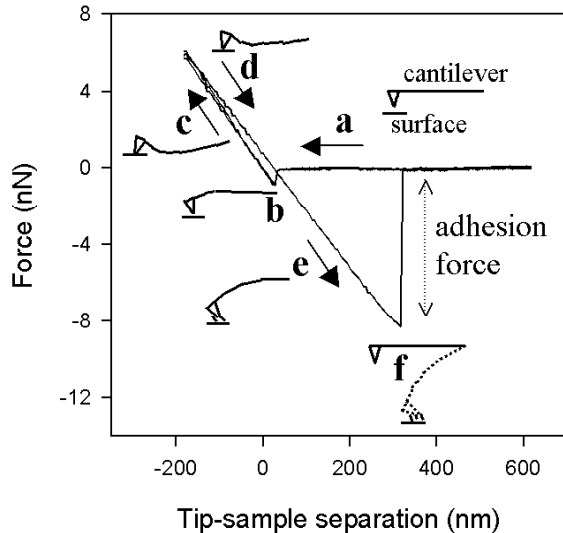


Figure 2: A typical force-distance curve obtained on a BOPP film surface with a cantilever having a spring constant of 0.03 N/m. Interaction between the tip and the surface at different distance is indicated by a-f. Arrows guide the eye to the direction of the movement of the tip. Adhesion force between the tip and sample due to their contact can be measured as shown in the force-distance curve.

Inserts in Figure 2 show the interaction between the tip and sample surface, which is detected by the deflection of the cantilever. There is no interaction between the tip and surface when the tip is far away from the surface (Insert a in Figure 2). When the tip is brought close enough to the surface there will be an attractive force between them. Usually, the gradient of the attractive force is much larger than the spring constant of the cantilever, so that the tip is snapped to the surface to make a contact between the tip and surface (b). Further extending the tip results in loading (repulsive) forces to the surface (c). This repulsive force is usually used as the feedback parameter for the AFM system to obtain surface morphology. Forces of a couple of nN are used in contact mode AFM. In the retracting cycle (d and e), because of the adhesion properties established after the contact between the tip and surface, the tip will not detach from the surface until the force used to pull the tip from the surface exceeds the adhesion force between them (f). This pull-off force can serve as a measure of the adhesion force between the tip and surface.^{13,15,43-47}

When the tip scans the surface in contact mode AFM, there is also a torsional movement of the cantilever that can be used to obtain further information on the interaction between the tip and surface. The measurement of this torsional movement

may be referred to as “lateral force” imaging.⁴⁸ Lateral force imaging in AFM is usually used to image the distribution of different friction forces on a surface.^{13,15,49-51} We also reported that lateral force imaging can enhance topographic features,¹⁴ which may be useful for surfaces where topographic images are difficult to obtain due to, for example, a large dynamic range for the height distribution of the sample surface. The arithmetical difference between the bi-directional lateral force images results in a friction force image, from which one is able to distinguish regions of higher hydrophilicity on the basis of increased interaction with the AFM tip. The direct output of the photodiode corresponding to the torsional movement of the cantilever, in units of nA, is the photo-induced current which was directly used to construct the lateral force image.

Dynamic force mode

Dynamic force (tapping or non-contact) mode AFM, in which a cantilever oscillated around its resonant frequency is used to probe surface features, was developed initially to eliminate surface degradation encountered in contact mode AFM, especially for soft materials.⁵²⁻⁵⁵ For dynamic force mode AFM, silicon cantilevers with a spring constant of ~ 40 N/m were used. The cantilever was $125 \mu\text{m}$ long, $30 \mu\text{m}$ wide and $3.7 \mu\text{m}$ thick. The tip apex radius was $10\text{-}20 \text{ nm}$. Because the variation of the oscillation amplitude is used in the feedback system, we show in Figure 3 the relative change of the oscillation amplitude of the cantilever versus distance between the tip and sample surface.

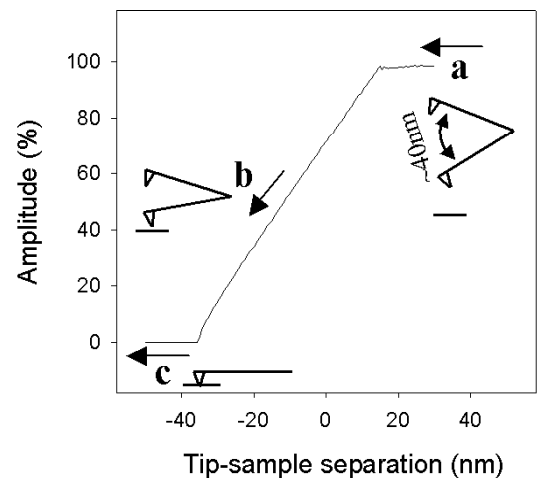


Figure 3: An amplitude-distance curve obtained on a BOPP film surface. Interaction between the tip and the surface at different tip-sample distance is indicated by inserts a-c. Arrows indicate the direction of the tip approaching to the sample surface.

Figure 3 shows that when the tip is far away from the surface (Insert a), the oscillation amplitude does not change, representing a “free space” situation. The amplitude decreases when the tip approaches close enough to the sample surface so that it “feels” attractive and/or repulsive forces (b). The

cantilever stops oscillating when the tip is brought in to mechanically contact the surface (c). Dynamic force mode AFM works by scanning the tip across the sample surface and adjusting the distance between the two through maintaining constant damped oscillation amplitude of the cantilever, usually at 50% of the free space oscillation.

All images were obtained in air with a typical relative humidity of about 50 %. AFM images consisted of 500 lines with 500 points per line. Scan rates for smaller (up to 4 μm square) and larger (over 5 μm square) areas were up to 10 and 50 $\mu\text{m}/\text{s}$, respectively. The images are in gray scale, where brighter areas represent higher areas.

Check tip performance

The BOPP film was used as a reference sample to check the performance of AFM tips. The simple criterion for judging a tip is whether it can image the nanometer-scale fiber-like network structure.^{18,19} When the tip is contaminated or damaged the tip becomes larger than the BOPP fibers and the image will be dominated by tip effect.

Commercial software (SPIP, Metrology Image ApS, Denmark) can be used to estimate the geometry of the tip with its “tip characterization” module, in which blind reconstruction algorithm^{37,40} is implemented. The algorithm is based on the fact that surface features sharper than the tip actually act as a probe to image the AFM tip itself. The advantage of this method is that it uses solely a given image to deduce the tip geometry.

We managed to obtain AFM images in the same area of BOPP film using the same tip before and after it was contaminated. The difference in these images was thus solely induced by the contaminants on the tip apex. The shape of the contaminated tip was estimated from the image collected using the contaminated tip. This estimated tip geometry was in turn used to dilate the image collected by the clean tip: the outcome should resemble the image collected by the contaminated tip. This way, one can test the software’s performance on estimating the tip shape from the image it collected.

Results and discussion

Morphology of BOPP film

AFM images obtained on BOPP films in an area of 20, 4 and 1 μm square are shown in Figures 4 (a), 4 (b) and 4 (c), respectively. The image in Figure 4 (a) shows the overall morphology of the BOPP film. The MD direction is nominally the vertical direction of the image shown in this and all other images included in this article. Running in the MD direction and approximately in the middle of the image is a barely visible scratch of only 1-2 nm deep. Those scratches are strictly in the MD direction and there is no end of a scratch ever observed through our extensive study on the morphology of the polymer film.^{14,15}

Though not appearing in the particular area shown in Figure 4 (a), there are veins (larger fibers) running nominally in the MD direction for the particular BOPP film we used.^{14,16} Figure 4 (b) shows that the BOPP film surface is characterized by a fiber-like network structure. The nanometer-scale network structure is revealed very clearly in a close-up image of the polymer film [Figure 4 (c)]. From the many AFM images we collected on the BOPP film, the apparent size of the fibers ranges from 10 to 40 nm. As we have discussed, the network structure of the polymer fibers reflects the drawing process in which the BOPP film had been formed by stretching the original film. A different draw ratio results in a different morphology for the fiber-like network structure.¹⁶

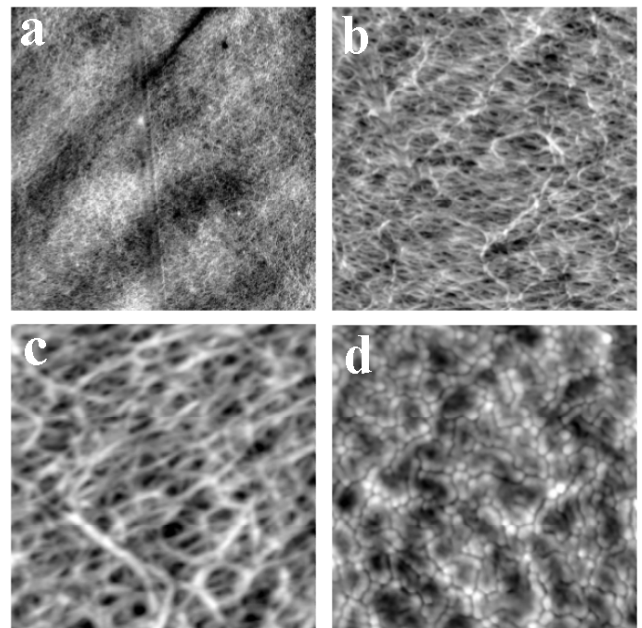


Figure 4: Typical AFM images of BOPP films in a scan area of (a) 20 μm \times 20 μm , (b) 4 μm \times 4 μm and (c) 1 μm \times 1 μm . Shown in (d) is an AFM image (scan area 1 μm \times 1 μm) obtained after sputtering a gold film of 30 nm thick on the BOPP film. The gray scales are 49, 29, 12 and 16 nm for (a), (b), (c) and (d), respectively

Shown in Figure 4 (d) is the morphology of a sputter coated gold film on a BOPP film. The morphology of the polymer surface has been altered significantly: the metal aggregates cover the surface but leave cracks that most likely correspond to the ridges of the fibers. This suggests that detailed surface structures of a polymer film can be easily altered if it is coated with a metal film. Although Figure 4 (d) shows a gold film of \sim 30 nm thick on a BOPP film, we confirmed that sputtering a gold film as thin as a couple of nm had also altered the fine fiber-like network structure. It is thus clear that AFM is an excellent tool capable of imaging the true surface morphology of the fine structure of polymer films.

We took a close look at the scratches found on the BOPP film, which are strictly in the MD direction. The scratches appear

to arise from mechanical deformation in the rolling process, where the BOPP film had to go through many rollers. It is imaginable that if there were tiny protrusions on the rollers, their presence would result in mechanical deformation on the film surface when rolling the film through the rollers. Such localised forces thus produced the scratches we observed.

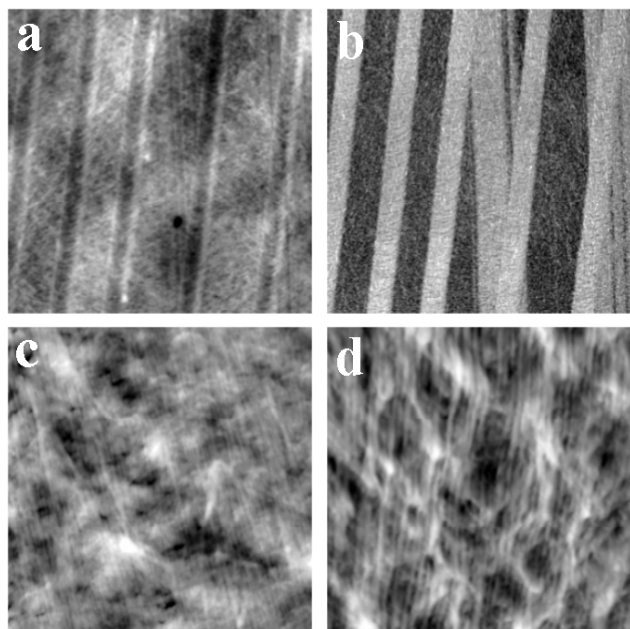


Figure 5: Topographic (a) and friction force (b) images (scan area $20\ \mu\text{m} \times 20\ \mu\text{m}$) for a BOPP film where native and stylus induced scratches are seen. Shown in (c) and (d) are topographic images (scan area $2\ \mu\text{m} \times 2\ \mu\text{m}$) for the native and stylus-produced scratches, respectively. The gray scales are 55, 19, and 15 nm for (a), (c) and (d), respectively. The gray scale for (b) is 5.38 to 7.85 nA, which is the (current) output of the photodiode for monitoring the friction force.

To prove that those “native” scratches are indeed caused by such a mechanical deformation imposed by the protrusions on the rollers, we have conducted experiments reproducing the scratches on the BOPP film surface by scanning a diamond-tipped stylus across the polymer film.¹⁵ Shown in Figures 5 (a) and 5 (b) are a contact mode AFM image and a friction force image, respectively, simultaneously obtained on a BOPP film. The diamond tip of $2.5\ \mu\text{m}$ in radius had been used to produce an array of scratches by scanning the surface at an applied force of 0.4 mN and a speed of $400\ \mu\text{m/s}$. The five scratches clearly seen in the topographic image [Figure 5 (a)] are those produced by the stylus. Those scratches are approximately 10 nm deep and 1450 nm wide, as compared to the much shallower, 1-2 nm deep “native” scratches, which happen to be in the same area. The “native” scratches can be barely seen in the topographic image [Figure 5 (a)] due to their shallowness compared to the surface roughness. As clearly shown in the friction force image [Figure 5 (b)], friction force measured on both the stylus-produced and “native” scratches are the same and larger than that on the “normal” areas. The

adhesion force, which is a measure of surface energy of the sample surface,¹⁵ measured on the scratched area is also larger than that on the “normal” area. Increase in surface energy on the scratched area is proposed to be due to a build up of extra free energy, which is transformed from part of the work done by the mechanical-scratching, in the form of increasing density and ordering of polymer molecular chains on the deformed surface.¹⁵

Shown in Figures 5 (c) and 5 (d) are close-up images for a “native” and a stylus-produced scratch, respectively. It is clear that the polymer strands were reoriented to the scratching direction. By comparing AFM images for the scratches and the “normal” areas, we found that the scratched areas show a much smaller corrugation height, indicating the scratched areas were also compressed. The contrast in the friction force image suggests a higher surface energy for the scratched areas. The higher surface energy is believed to be due to the increased density and ordering of the polymer strands in the mechanically deformed areas.¹⁵

We have conducted scratch tests on the polymer surface using the diamond tip with different applied stylus forces. Because the polymer surface is plastically deformed, the scratch width increases almost linearly with the applied force.⁵⁶ As shown in Figures 5 (a) and 5 (b), the stylus-produced scratches have the same width because the conditions to make them are identical. In contrast, the “native” scratches observed in this area and other areas (not shown) have various widths, suggesting that the length and/or the size of the protrusions on the rollers are diverse. One can expect that the “native” scratches such as those observed for the BOPP film we used will probably disappear with the removal of such protrusions from the rollers.

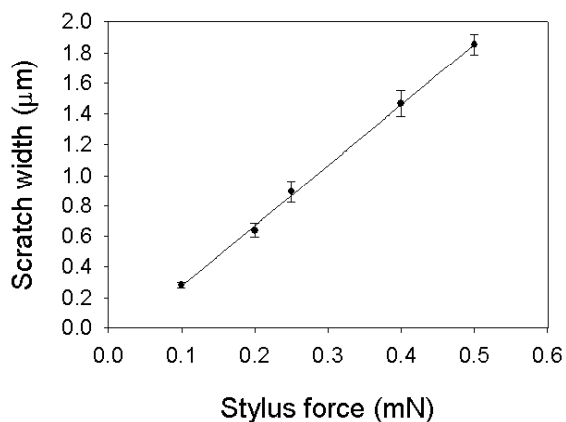


Figure 6: Width of scratches produced by a diamond-tipped stylus as a function of the applied force.

UV/ozone and ozone-only treatments

Shown in Figure 7 (a) is an AFM image obtained on a 1-min UV/ozone treated BOPP film. Adhesion force measurement showed a clear increase in surface energy on this treated surface,¹⁵ indicating that the chemistry of the surface was

modified by the treatment. This adhesion force measurement using AFM¹⁵ is consistent with previous measurements using X-ray photoelectron spectroscopy (XPS) and contact angle method, in which they showed an uptake of oxygen and a decrease in contact angle, respectively, for 1-min UV/ozone treated BOPP samples.²⁰

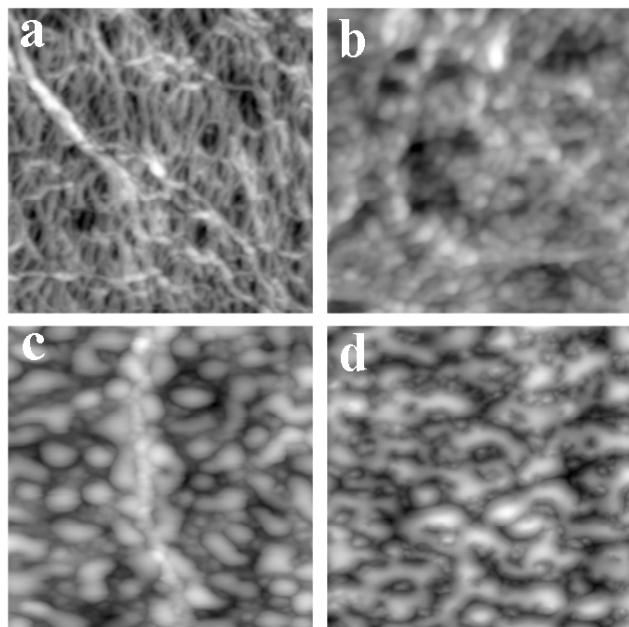


Figure 7: Topographic images (scan area $2 \mu\text{m} \times 2 \mu\text{m}$) for BOPP films subjected to UV/ozone treatment for (a) 1 min, (b) 4 min, (c) 15 min and (d) 45 min. The gray scales are 33, 31, 32 and 39 nm for (a), (b), (c) and (d), respectively.

However, the fiber-like feature remains after this 1-min UV/ozone treatment. It is thus believed that there are oxygen-containing functional groups formed on the surface, which accounts for the observed chemistry change on the surface. The oxidation is thus insufficient for breaking the polymer chains to form low molecular weight oxidized material (LMWOM).

After an UV/ozone treatment for 4 min [Figure 7 (b)], the surface morphology changed completely: nodule-like features emerged. This morphology change is the result of oxidation of the polymer surface, resulting in the formation of LMWOM including carbonyls, carboxylic acids, hydroxyl-group and many other oxygen-related groups.²⁰ Increasing treatment time resulted in the formation of larger mounds on the surface. Shown in Figure 7 (c) is an AFM image for a 15-min UV/ozone treated BOPP film surface. Compared to the nodule-like features seen on the 4-min treated sample, the 15-min treated sample shows elongated droplets. It is reasonable to assume that as one increases the treatment time, more LMWOM is produced. The greater volume of LMWOM allows it to accumulate to form larger droplets.¹⁷

Morphology changes and the formation of LMWOM have been clearly shown by AFM. Another aspect of the formation of LMWOM is the increase in water wettability as previously determined from contact angle measurements.²⁰ An additional advantage in using AFM to investigate modified polymer surfaces is that it also provides information on changes in the adhesion force at the surface. The adhesion force was found to increase with increasing treatment time.^{13,17} The increase in adhesion force indicates an increase in surface energy. The surface energy increase for the UV/ozone treated BOPP film is a direct result of the oxidation of the polymer surface, resulting in polar oxidized materials.²⁰

An extended UV/ozone treatment for 45 min resulted in yet another change in morphology. As shown in Figure 7 (d), the surface morphology is now characterized by connected droplets. This suggests that, as more LMWOM is produced, the resultant droplets contact and coalesce. The morphology shown in Figure 7 (d) indicates a relatively small difference of surface energy between the underlying surface and the droplets because the droplets have spread out on the underlying surface.

The oxidized material (LMWOM) forming the droplets is found to be water washable, suggesting that they are soluble in water. However, washing does not restore the fiber-like structure of the pristine BOPP film, indicating that the underlying surface is covered by moderately oxidized materials that are insoluble in water.¹⁷ Because this underlying surface still displays higher surface energy, the improvement of wettability is preserved even after washing the UV/ozone treated surface.

It has been established that UV/ozone treatment modifies the polymer surface quickly. UV irradiation is believed to provide reactive atomic oxygen through photo-decomposition of ozone.²⁰ XPS has been used to measure the uptake of oxygen on the ozone and UV/ozone treated BOPP film samples. O/C ratios calculated from the XPS measurement show that the oxygen uptake is much lower and slower for the ozone treatment than for the UV/ozone treatment.²⁰ We have reported preferential oxidation in the scratched area for UV/ozone treatment, as judged from the difference in the size of the mounds between the scratched and “normal” areas.¹⁷ In order to see how different the oxidation would be if no such reactive atomic oxygen were generated, we conducted experiments using ozone only to treat the polymer film. Shown in Figure 8 are AFM images for BOPP films subjected to ozone exposure (the ozone flow rate was 5000 scfm) without UV irradiation for different periods of time.

Figure 8 (a) is a reference image of a BOPP film without the treatment. As shown in Figure 8 (b), BOPP films subjected to 10-min ozone treatment shows no significant change in morphology. Even after an ozone treatment for 30 min, the fiber-like network structure is still visible [Figure 8 (c)]. After exposing a BOPP film to ozone for 45 min, the surface

morphology of the polymer film starts showing the formation of nodules [Figure 8 (d)]. Compared to UV/ozone treatment, the ozone only treatment is much slower in modifying the morphology of the polymer surface. Therefore, UV irradiation plays an important role in the oxidation of the polymer surface for the UV/ozone treatment. As investigated from other techniques, atomic oxygen generated through a photo-decomposition process induced by UV irradiation is the key for quickly modifying the polymer surface.²⁰

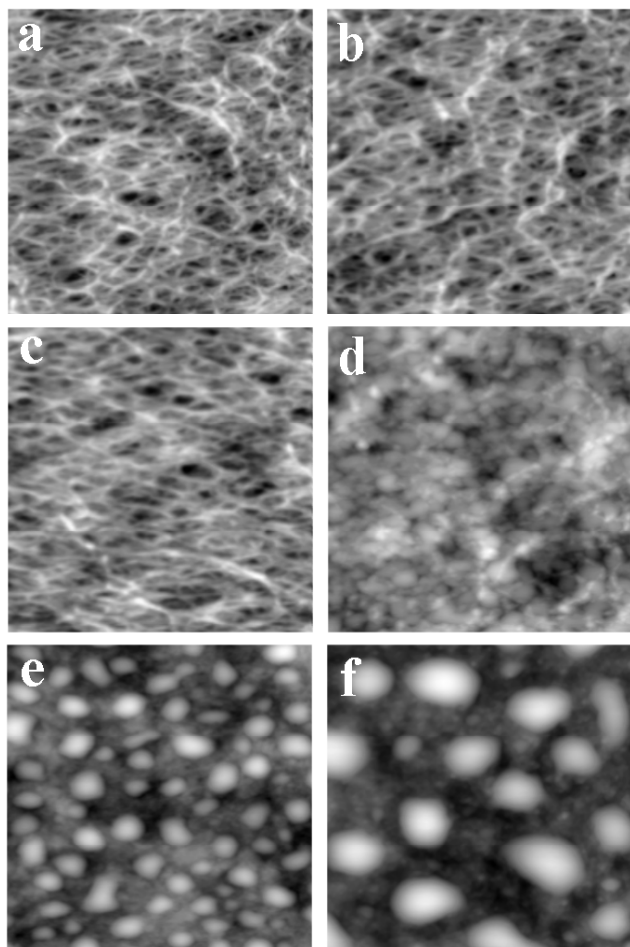


Figure 8: Topographic images (scan area $2 \mu\text{m} \times 2 \mu\text{m}$) for BOPP films subjected to ozone only treatment for (a) 0 min, (b) 10 min, (c) 30 min, (d) 45 min, (e) 60 min and (f) 120 min. The gray scales are 25, 26, 18, 21, 25 and 43 nm for (a), (b), (c), (d), (e) and (f), respectively.

When the ozone treatment time was increased to 60 min, well-separated droplets emerge on the polymer surface [Figure 8 (e)]. By comparing Figures 7 (c) and 8 (e), one can see that the size of the droplets for the 15-min UV/ozone treated and 60-min ozone treated surface is similar. However, the ozone treated surface shows round and well-separated droplets, in contrast to the elongated and more closely packed droplets on the UV/ozone treated surface. Figure 8 (f) is an AFM image for the morphology of a BOPP film treated by ozone for 120 min, showing the formation of large droplets that are separated

from each other. It appears that the droplets induced by ozone treatment grow with increasing treatment time but remain separated. This is in contrast to those observed for UV/ozone treated samples, as shown in Figure 7 (d). The difference in morphology suggests that the oxidized materials from the two different treatments may be different.

Shown in Figure 9 are two AFM images for the ozone only treatment of BOPP films (the ozone flow rate was 2000 sccm), displaying preferential oxidation in the scratched area as evidenced by the formation of droplets in the scratched area, but not in the “normal” area. The scratched area is at the left hand side of the image shown in Figure 9 (a). Differences in the oxidation in the scratched and “normal” areas are clearly depicted in the image. Figure 9 (b) shows a close-up image for the scratched area at the left hand side and the “normal” area at the right hand side, respectively. We confirmed that the mounds produced by ozone only treatment are also removed by water washing, similar to those produced by UV/ozone treatment.

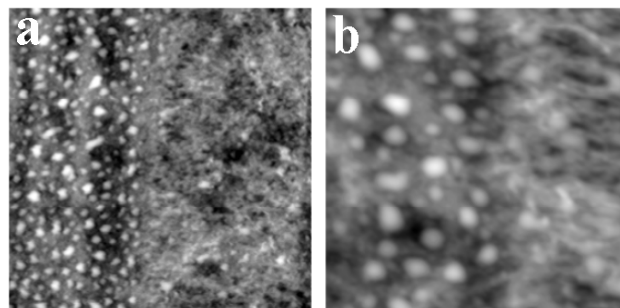


Figure 9 Topographic images for ozone only treated BOPP film in an area of (a) $5 \mu\text{m} \times 5 \mu\text{m}$ and (b) $2 \mu\text{m} \times 2 \mu\text{m}$, showing preferential oxidation in scratched area. The gray scales are 36 and 20 nm for (a) and (b), respectively

AFM measurements show that the change in the surface structures is accompanied by a change in surface energy.¹⁵ Increase in surface energy caused by the mechanical deformation may have an implication for understanding the surface modifications of polymer. Figure 9 shows preferential oxidation in the scratched area. This is attributed to the fact that the scratched area has a higher initial surface energy, making it more amenable to oxidation.

Check tip performance using the BOPP film

Shown in Figure 10 (a) is an AFM image obtained on a BOPP film using a clean tip, reflecting the true morphology characterized by the fiber-like network structure. When damaged or contaminated AFM tips were used, the fiber-like features are no longer seen in the AFM images [Figures 10 (b) to 10 (d)]. The three images are obviously dominated by three different tip shapes. AFM images in Figure 11 strongly suggest that the BOPP film can be used as a reference sample to check the performance of an AFM tip. The criterion is simple and straight forward: if the fiber-like features are

revealed by an AFM tip, then the tip quality is sufficient to collect “true” images.^{18,19} An AFM tip can be easily contaminated or damaged depending on the chemical and mechanical properties of the sample surface it scans.⁵⁷ It is therefore desirable to adopt a simple qualifying method such as the one using BOPP film to check the performance of AFM tips.

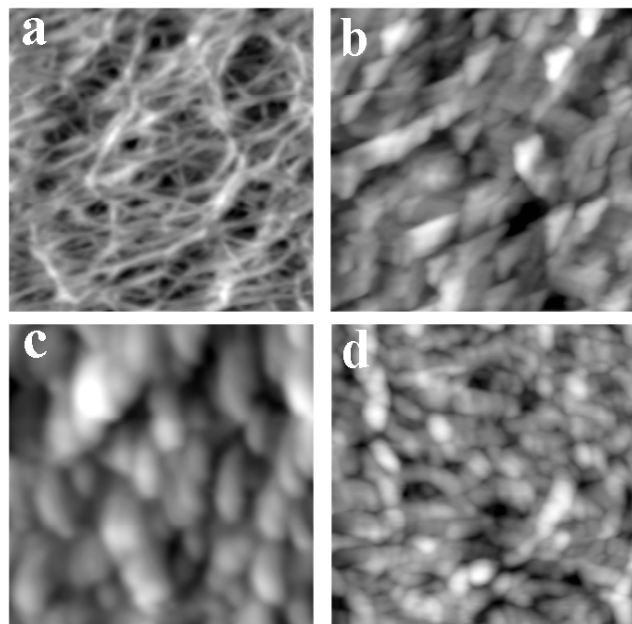


Figure 10: Topographic images (scan area $1 \mu\text{m} \times 1 \mu\text{m}$) for BOPP films obtained by (a) a clean tip, (b) a damaged tip, (c) another damaged tip and (d) a contaminated tip. The gray scales are 19 nm for all images.

In order to prove that BOPP film is indeed useful for checking AFM tip performance, we managed to image the same area using the same tip when it was clean, after it had been contaminated and then after it was cleaned again. That way, any change in the AFM images obtained would be solely due to the contamination on the tip apex. Two tips were contaminated by scanning two specially prepared samples.¹⁹ Shown in Figure 11 are two sets of AFM images for two different contaminated tips. The first set of AFM images shown in Figures 11 (a), 11 (c) and 11 (e) are obtained on the same area using a tip when it was clean, contaminated and re-cleaned, respectively. The tip used for Figure 11 (c) was contaminated by scanning a sample surface that was UV/ozone treated followed by water washing.^{18,19} It is clear that the image collected by the contaminated tip is dominated by tip effect [Figure 11 (c)].

We cleaned the contaminated tip by pushing it into the polymer film, and its cleanliness is evidenced in AFM image shown in Figure 11 (e). An amplitude-distance curve such as the one shown in Figure 3 is used to control as how deeply the tip is pushed into the polymer surface. The depth can be controlled by counting from the distance where the cantilever

stopped oscillating. In the course of pushing the tip into the polymer film, its behaviour may be reflected in the amplitude-distance curve as it is being removed from the tip apex.¹⁸

Shown in Figure 11 (b), 11 (d) and 11 (f) are AFM images using another contaminated tip on another BOPP film, when the tip was clean, contaminated and cleaned, respectively. By comparing Figures 11 (c) and 11 (d), it is clear that this tip was contaminated differently from the one described above. In fact, this tip was contaminated by being scanned on an organic acid⁵⁸ coated Si substrate.¹⁹ Once again, the use of the BOPP film to check the AFM tip performance and to clean the contaminated tip was successful.

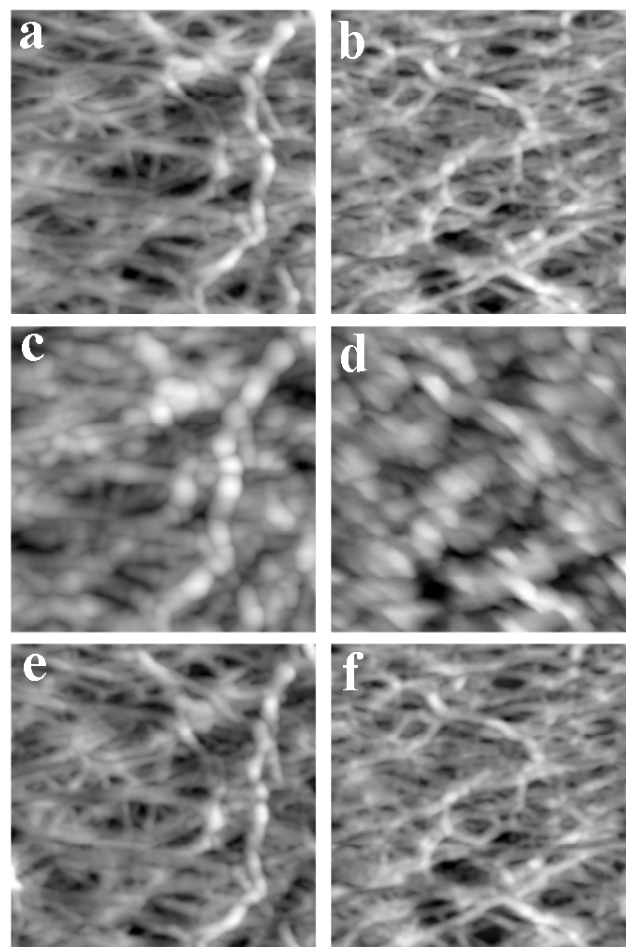


Figure 11: Topographic images (scan area $1 \mu\text{m} \times 1 \mu\text{m}$) obtained on the same BOPP area when the same AFM tip was (a) clean, (c) contaminated and (e) cleaned. Another example using a differently contaminated tip is shown in (b), (d) and (f). The gray scales are 31, 24, 29, 15, 29 and 24 nm for (a), (b), (c), (d), (e) and (f), respectively.

For contaminated tips used to collect AFM images in Figure 11, pushing it into the polymer film cleans it. If a tip was damaged, pushing the tip into the polymer would not result in a better tip. If uncertain about whether or not a tip is contaminated or damaged, UV/ozone treatment of the tip for

half an hour usually answers the question. This is because most organic contamination would be removed by the UV/ozone treatment. Based on this procedure we identified that the tips corresponding to images shown in Figures 10 (b) and 10 (c) were damaged and the one to Figure 10 (d) was contaminated.

We take advantage of our ability to image the same area of the BOPP film before and after the same tip was contaminated to test commercial software in which the algorithm of blind reconstruction for extracting the tip shape was implemented. The difference in such AFM images is solely due to the tip contamination. The contaminated tip can be estimated from the image it collected. Shown in Figures 12 (a) and 12 (b) are topographic images for the geometry of the tip estimated from Figures 11 (c) and 11 (d), respectively. According to the tip shape estimated from the image in Figure 11 (c), the upper bond of the contaminant on the tip is basically round and has a radius of ~ 80 nm, comparing to the nominal radius of 10-20 nm for a clean tip.

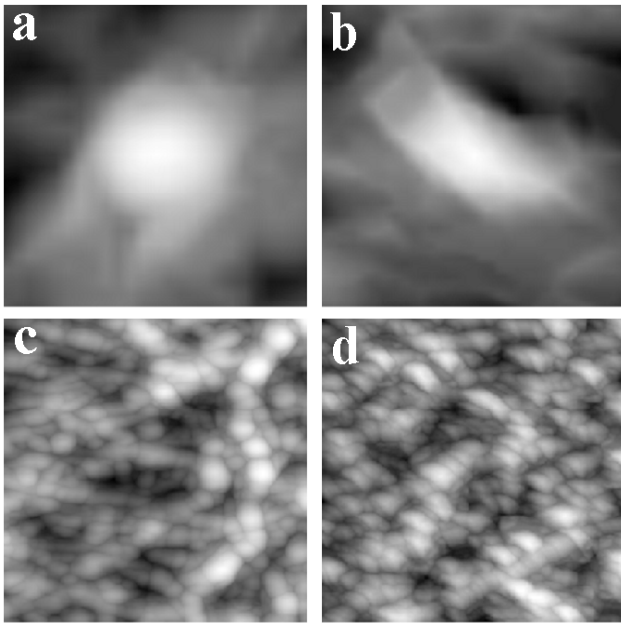


Figure 12: Shown in (a) and (b) are geometry of the contaminated tips estimated from the images of Figures 12 (c) and (d), respectively. The images in (c) and (d) are images dilated from Figures 12 (a) and 12 (b) using the tip shown in (a) and (b), respectively. The lateral dimensions for (a) and (b) are 168 nm; the gray scales are 24 and 14 nm for (a) and (b), respectively.

Figure 12 (b) shows a differently shaped contaminant estimated from Figure 11 (d). This contaminant is elongated 90 nm across the elongated direction. The apparent height for the contaminant shown in Figures 12 (a) and 12 (b) is 20 and 14 nm, respectively. This is most likely an underestimated height for the contaminant because the limited height of the surface features of the BOPP film only images the top of the

tip. The flat outlying areas in Figures 12 (a) and 12 (b) are artefacts reflecting this limitation.

The blind reconstruction algorithm extracts the AFM tip shape solely from the AFM image collected by the tip. Dilation is a mathematical operation that convolutes the tip effect to an existing image, which simulates the AFM imaging mechanism. Based on dilation of a tip geometry into an image and our ability of imaging the same area of the BOPP film surface using the same tip before and after it was contaminated, we have proposed a simple way to test blind reconstruction: comparison of the AFM image collected using the contaminated tip [Figures 11 (c) or 11 (d)] and the dilated image [Figures 12 (c) or 12 (d)] from the image collected using the clean tip [Figures 11 (a) or 11 (b)]. If the estimation of the contaminated tip geometry is reasonable, then one expects to be able to use the estimated tip geometry to dilate the image collected using the clean tip to obtain an image resembling one collected using the contaminated tip. Shown in Figure 12 (c) and 12 (d) are dilated images from Figures 11 (a) and 11 (b) using the estimated contaminated tip geometry shown in Figures 12 (a) and 12 (b), respectively. It is clear that the dilated images resemble the images collected using the contaminated tips. Therefore, blind construction algorithm successfully extracts the geometry of the contaminated tip.

Conclusions

Nanometer-scale morphology of a BOPP film and its surface modification by UV/ozone and ozone only treatments were investigated using AFM. Surface modification by UV/ozone treatment is much faster than that by ozone only treatment, consistent with the oxygen-uptake measurements by XPS technique. Scratches produced by force-controlled diamond-tipped stylus show a linear increase of scratch width with the applied force. It is therefore concluded that the native scratches on the polymer film are due to mechanical deformation occurring in the rolling process in which protrusions on rollers are most likely the source for such mechanical forces. Preferential oxidation was observed on scratched areas, indicating they are more amenable to surface modification by ozone or UV/ozone treatment.

The nanometer-scale fiber-like network structure of the BOPP film surface found use in checking AFM tip performance. This is because the size of the fibers is close to the apex radius of clean tips but smaller than a contaminated tip. The ability to collect images of the same areas using the same tip when it was clean and contaminated provided a simple way to test the blind reconstruction algorithm, which allows one to attract tip geometry solely from the image it collected.

References

¹G. Binnig, H. Rohrer, Ch. Gerber, and E. Weibel, *Appl. Phys. Lett.*, 40, 178 (1982).

- ²G. Binnig, H. Rohrer, Ch. Gerber, and E. Weibel, *Phys. Rev. Lett.*, 49, 57 (1982).
- ³G. Binnig, C.F. Quate, and Ch. Gerber, *Phys. Rev. Lett.*, 56, 930 (1986).
- ⁴M. Aboulfaraj, B. Ulrich, A. Dahoun, and C. G'Sell, *Polymer*, 34, 4817 (1993).
- ⁵R.A. Campbell, P.J. Phillips, and J.S. Lin, *Polymer*, 34, 4809 (1993).
- ⁶W. Stocker, M. Schumacher, S. Graff, J. Lang, J.C. Wittmann, A.J. Lovinger, and B. Lotz, *Macromolecules*, 27, 6948 (1994).
- ⁷D. Snetivy and G.J. Vancso, *Polymer*, 35, 461 (1994).
- ⁸V.V. Tsukruk and D.H. Reneker, *Macromolecules*, 28, 1370 (1995).
- ⁹G. Castelein, G. Coulon, and C. G'Sell, *Polym. Eng. Sci.*, 37, 1694 (1997).
- ¹⁰S. Hild, W. Gutmannsbauer, R. Luthi, J. Fuhrmann, and H.-J. Gruntherodt, *J. Polym. Sci.: Polym. Phys.*, 34, 1953 (1996).
- ¹¹R.M. Overney, R. Luthi, H. Haefke, J. Frommer, E. Meyer, H.-J. Gruntherodt, S. Hild, and J. Fuhrmann, *Appl. Surf. Sci.*, 64, 197 (1993).
- ¹²M. Strobel, V. Jones, C.S. Lyons, M. Ulsh, M.J. Kushner, R. Dorai, and M.C. Branch, *Plasmas Polym.*, 8, 61 (2003).
- ¹³H.-Y. Nie, M.J. Walzak, B. Berno, and N.S. McIntyre, *Appl. Surf. Sci.*, 144-145, 627 (1999).
- ¹⁴H.-Y. Nie, M.J. Walzak, N.S. McIntyre, and A.M. EL-Sherik, *Appl. Surf. Sci.*, 144-145, 633 (1999).
- ¹⁵H.-Y. Nie, M.J. Walzak, B. Berno, and N.S. McIntyre, *Langmuir*, 15, 6484 (1999).
- ¹⁶H.-Y. Nie, M.J. Walzak, and N.S. McIntyre, *Polymer*, 41, 2213 (2000).
- ¹⁷H.-Y. Nie, M.J. Walzak, and N.S. McIntyre, in *Polymer Surface Modification: Relevance to Adhesion*, Vol. 2, edited by K.L. Mittal (VSP, Utrecht, The Netherlands, 2000), p. 377.
- ¹⁸H.-Y. Nie and N.S. McIntyre, *Langmuir*, 17, 432 (2001).
- ¹⁹H.-Y. Nie, M.J. Walzak and N.S. McIntyre, *Rev. Sci. Instrum.*, 73, 3831 (2002).
- ²⁰M.J. Walzak, S. Flynn, R. Foerch, J.M. Hill, E. Karbasheski, A. Lin, and M. Strobel, *J. Adhesion Sci. Technol.*, 9, 1229 (1995).
- ²¹J.M. Hill, E. Karbasheski, A. Lin, M. Strobel, and M.J. Walzak, *J. Adhesion Sci. Technol.*, 9, 1575 (1995).
- ²²M. Strobel, M.J. Walzak, J.M. Hill, A. Lin, E. Karbasheski, and C.S. Lyons, *J. Adhesion Sci. Technol.*, 9, 365 (1995).
- ²³D. Vick, M. J. Brett and K. Westra, *Thin Solid Films*, 408, 79 (2002), and references therein.
- ²⁴C.J. van Oss, M.K. Chaudhury, and R.J. Good, *Sep. Sci. Technol.*, 24, 15 (1989).
- ²⁵S. Wu, *Polymer Interface and Adhesion* (Marcel Dekker, New York, 1982), Chapter 5.
- ²⁶H. Schonhorn and L.H. Sharpe, *J. Polym. Sci. B*, 3, 235 (1965).
- ²⁷W. Brostow, J. Kubat, and M.M. Kubat, in *Physical Properties of Polymers Handbook*, edited by J.E. Mark (American Institute of Physics, New York, 1996), p. 331.
- ²⁸L.M. Zhang, D. Uttamchandani, and B. Culshaw, *Sensors and Actuators A*, 29, 79 (1991).
- ²⁹K.E. Petersen, *Proceedings of the IEEE*, 70, 420 (1982).
- ³⁰J.J. Wortman and R.A. Evans, *J. App. Phys.*, 36, 153 (1965).
- ³¹P. Markiewicz and M.C. Goh, *Langmuir*, 10, 5 (1994).
- ³²J. Vesenka, R. Miller, and E. Henderson, *Rev. Sci. Instrum.*, 65, 2249 (1994).
- ³³J.S. Villarrubia, *Surf. Sci.*, 321, 287 (1994).
- ³⁴P. Markiewicz and M.C. Goh, *Rev. Sci. Instrum.*, 66, 3186 (1995).
- ³⁵P. Markiewicz and M.C. Goh, *J. Vac. Sci. & Technol. B*, 13, 1115 (1995).
- ³⁶S. Dongmo, M. Troyon, P. Vautrot, E. Delain, and N. Bonnet, *J. Vac. Sci. & Technol. B*, 14, 1552 (1996).
- ³⁷P.M. Williams, K.M. Shakesheff, M.C. Davies, D.E. Jackson, C.J. Roberts, and S.J.B. Tendler, *J. Vac. Sci. & Technol. B*, 14, 1557 (1996).
- ³⁸J. Vesenka, T. Marsh, R. Miller, and E. Henderson, *J. Vac. Sci. & Technol. B*, 14, 1413 (1996).
- ³⁹M.F. Tabet and F.K. Urban, *J. Vac. Sci. & Technol. B*, 15, 800 (1997).
- ⁴⁰J.S. Villarrubia, *J. Res. Natl. Inst. Stan.*, 102, 425 (1997).
- ⁴¹L.S. Dongmo, J.S. Villarrubia, S.N. Jones, T.B. Renegar, M. Postek, and J.F. Song, *Ultramicroscopy*, 85, 141 (2000).
- ⁴²B.A. Todd and S.J. Eppell, *Surf. Sci.*, 491, 473 (2001).
- ⁴³H.A. Mizes, L.-G. Loh, R.J. Miller, S.K. Ahuja, and E.F. Grabowski, *Appl. Phys. Lett.*, 59, 2901 (1991).
- ⁴⁴M. Radmacher, M. Fritz, J.P. Cleveland, D.A. Walters, and P.K. Hansma, *Langmuir*, 10, 3809 (1994).
- ⁴⁵G. Toikka, R.A. Hayes, and J. Ralston, *J. Colloid Interface Sci.*, 180, 329 (1996).
- ⁴⁶E.W. van der Vegte and G. Hadziioannou, *Langmuir*, 13, 4357 (1997).
- ⁴⁷K. Feldman, T. Tervoort, P. Smith, and N.D. Spencer, *Langmuir*, 14, 372 (1998).
- ⁴⁸G. Meyer and N. Amer, *Appl. Phys. Lett.*, 57, 2089 (1990).
- ⁴⁹R.M. Overney, E. Meyer, J. Frommer, D. Brodbeck, R. Luthi, L. Howald, H.-J. Guntherodt, M. Fujihira, H. Takano, and Y. Goto, *Nature*, 58, 133 (1992).
- ⁵⁰Y.F. Dufrene, W.R. Barger, J.-B.D. Green, and G.U. Lee, *Langmuir* 13, 4779 (1997).
- ⁵¹M. Motomatsu, H.-Y. Nie, W. Mizutani, and H. Tokumoto, *Jpn. J. Appl. Phys.*, 33, 3775 (1994).
- ⁵²Q. Zhong, D. Inniss, K. Kjoller, and V.B. Elings, *Surf. Sci.*, 290, L688 (1993).
- ⁵³J.P. Spatz, S. Sheiko, M. Moller, R.G. Winkler, P. Reineker, and P. Marti, *Nanotechnology*, 6, 40 (1995).
- ⁵⁴J. Tamayo and R. Garcia, *Langmuir*, 12, 4430 (1996).
- ⁵⁵N.A. Burnham, O.P. Behrend, F. Oulevey, G. Gremaud, P.-J. Gallo, D. Gourdon, A.J. Kulik, H.M. Pollock, and G.A.D. Briggs, *Nanotechnology*, 8, 67 (1997).
- ⁵⁶B.Y. Du, M.R. VanLandingham, Q.L. Zhang and T.B. He, *J. Mater. Res.*, 16, 1487 (2001).
- ⁵⁷B. Skarman, L.R. Wallenberg, S.N. Jacobsen, U. Helmersson, and C. Thelander, *Langmuir*, 16, 6267 (2000).
- ⁵⁸H.-Y. Nie, M.J. Walzak, and N.S. McIntyre, *Langmuir*, 18, 2955 (2002).